Effect of silica nanoparticles on compressive properties of an epoxy polymer

A. Jumahat[a,b], C. Soutis[a,*], F. R. Jones[c] and A. Hodzic[a]

[a] Department of Mechanical Engineering, Aerospace Engineering, University of Sheffield, Sheffield S1 3JD, UK

[b] Faculty of Mechanical Engineering, Universiti Teknologi MARA, 40450 Shah Alam, Selangor, Malaysia

[c] Department of Engineering Materials, University of Sheffield, Sheffield S1 3JD, UK

ABSTRACT

The effect of nanosilica on compressive properties of an Epikote 828 epoxy at room temperature was studied. A 40 wt% nanosilica/epoxy masterbatch (nanopox F400) was used to prepare a series of epoxy based nanocomposites with 5-25 wt% nanosilica content. Static uniaxial compression tests were conducted on cubic and cylindrical specimens to study the compressive stress-strain response, failure mechanisms and damage characteristics of the pure and nanomodified epoxy. It was found that the compressive stiffness and strength were improved with increasing nanosilica content without significant reduction in failure strain. The presence of nanosilica improved ductility and promoted higher plastic hardening behaviour after yielding in comparison with the unmodified resin system. This result suggested that nanoparticles introduced additional mechanisms of energy absorption to enhance the compressive properties without reducing the deformation to failure.

Keywords: Nanocomposites; Epoxy matrix; Compressive properties

1. Introduction

Composite materials made of epoxy matrices reinforced with high strength, high modulus continuous carbon fibres of 5-7 μm filament diameter are the most versatile materials used in the development of modern aircraft and automobile structures [1]. Carbon fibre reinforced polymer (CFRP) composites offer high strength and stiffness to weight ratios as well as good

* Corresponding author. Tel.: +44(0)114 222 7811, Fax: +44(0)114 222 7729. *Email address:* c.soutis@sheffield.ac.uk

resistance to fatigue and corrosion properties [2, 3]. However, the most serious drawback associated with these materials is their weak compressive strength due to brittle behaviour of both carbon fibre and epoxy resin. This weakness leads to low damage resistance and tolerance of the composite structure. High strain carbon fibre and toughened epoxy resin have been developed to improve the mechanical performance of CFRP composites in recent years. However, attempts to improve failure strain and strength of the carbon fibre often lead to reduced stiffness and vice versa [3].

The tensile behaviour of CFRP composites is mostly dominated by fibre properties. However, in compression, the fibre-matrix interface and matrix properties play an important role in providing lateral support to the fibre. Scanning electron micrographs revealed that the failure of the unidirectional CFRP composite laminate was initiated by fibre microbuckling and subsequent plastic kinking of the material [4]. Therefore the development of stiffer and tougher matrices is aimed at delaying fibre microbuckling, extend plastic hardening behaviour of the matrix and give better resistance to crack initiation and propagation. As a result, this will improve the overall matrix-dominated properties of the CFRP composites such as shear and compressive strength, compression after impact and open hole compression. This means that it will produce less notch sensitive composite systems. However, higher toughness is frequently coupled with lower modulus which leads to lower compressive strength of the composite. For instance, rubber and elastomers show ductility to some degree and are less rigid than the polymer matrix. These serve as excellent toughening agents in matrices. Rubber tends to improve the toughness of the epoxy by preventing the propagation of cracks and boosting the strain capability. Rubber particles induce the formation of microvoids and activate the yielding processes of the matrix [5]. A substantial amount of energy is dissipated within the plastic zone near the crack tip. This contributes to the tougher matrix [6]. However, the increase in toughness of the epoxy-rubber matrix is accompanied by a reduction in elastic modulus, strength, creep resistance and the thermal stability of the composite [7-9]. Moreover, a lower compressive strength of the CFRP system was observed in [10] because the micron-sized particles formed a compliant interface (or interleaf) between fibre plies which minimised the capability of the epoxy to support the fibres. The use of the other conventional additives in epoxy resin which results in similar drawbacks are core shell particles, glass beads, ceramic, hyper-branched polymers and other micron-sized inorganic fillers [11-15].

In contrast to those toughened systems which have been discussed above, fracture toughness can be increased without sacrificing other important characteristics by inclusion of

thermoplastics particles into epoxy matrix (or via solution blend). Thermoplastic-filled epoxy polymers have better thermal and mechanical properties compared to the pristine polymers. These have been reported by several researchers, eg., [8-10, 16-17]. The high-performance thermoplastic materials, such as polysulfone, polyether sulfone, polyether imide and polyimide, have been used to modify epoxy resins. However, the rate of increase in viscosity of the epoxy-thermoplastic blend is much higher than the rate of increase in toughness of the resultant matrix [18]. The exponential increase in viscosity limits the process ability and handle ability of the matrix. For instance, the thermoplastic toughened epoxy Cycom 977-2 resin has a viscosity of more than 500 Pa.s at 65^{o}C while the Cycom 977-20, high molecular weight epoxy which has no thermoplastic, has a 0.5–1 Pa.s viscosity at the same temperature. Therefore the optimum toughness is always sacrificed to maintain the process ability of the resin. Other than that, the large residual stresses generated in the processing of high performance thermoplastic reinforced polymer composites as discussed in [19] need to be considered. The residual stresses occurred due to gradients in cooling rate, thermal shrinkage mismatch and material density.

The latest advanced polymer technology is polymer nanocomposites. It consists of a polymeric material, such as thermoplastics, thermosets or elastomers, mixed with a nanoscale-filler. The selection of a particular polymer matrix and the appropriate nanoparticles depends on the desired properties of the finished products and their specific application. There are several types of nanoparticles commercially available and commonly used for developing epoxy-nanocomposites, such as montmorillonite organoclay, nanosilica, carbon nanotubes and nanofibres. The incorporation of nanofiller into the epoxy matrix enhances toughness, Young's modulus and thermal resistance have been reported by several researchers [20-24]. However, polymer nanocomposites have not yet reached their full potential as advanced engineering materials due to several challenges such as:

(a) selection of processing method to uniformly disperse the nanoparticles in the matrix (nanoparticles aggregate within the polymer matrix)
(b) viscosity increase with nanoparticle content
(c) selection of nanomaterial which is compatible with the polymer matrix to create strong interfacial interaction between them. This includes type of surface treatment required.

Agglomerated nanoparticle in the matrix introduces local stress concentration and a weak particle-matrix adhesion reduces the capability of load transfer between them. These lead to a premature failure of the polymer and thus reduce its strength and strain to failure.

In this study, specimens with highly dispersed nanosilica particles in the Epikote 828 epoxy were fabricated. The spherical silica nanoparticles were supplied as a colloidal sol in the diglycidyl ether of bisphenol A (DGEBA) epoxy, Nanopox F400, by Nanoresins AG, Geesthacht, Germany. The particles were synthesised from aqueous sodium silicate solution which then underwent organosilane and matrix exchange surface treatment processes to produce a 40 wt% nanosilica-epoxy masterbatch [24]. The viscosity of the F400 resin is relatively low due to fully dispersed nanosized silica. A series of nanocomposites with 5-25 wt% nanosilica content was prepared. The degree of dispersion of the nanosilica in the modified resin was evaluated and the volume fraction was determined. The mechanical performance of the nanocomposites was characterised based on their compressive properties at room temperature. In addition, the effect of specimen shape and geometry on compressive stress-strain response, failure mechanisms and damage characteristics was also studied.

2. Experimental Details

2.1 Fabrication of nanosilica-filled Epikote 828

The pure resin used for the experiment was a mixture of 100 parts, by mass, Epikote 828 (DGEBA) (supplied by Robnor Resins, UK), 90 parts HY906 which is a curing agent type 1-methyl-5-norbornene-2,3-dicarboxylic anhydride (NMA) (supplied by Robnor Resins, UK) and 1 part DY062, Benzyldimethylamine (BDMA) (supplied by Huntsman Advanced Materials Ltd., UK) which is used as the accelerator. In order to prepare a series of nanocomposites with 5-25 wt% nanosilica content, the Epikote 828 resin was mechanically mixed with Nanopox F400 nanosilica/DGEBA masterbatch in a heated oil bath of 80^{o}C for 2 h. The mixture was degassed in a vacuum oven at 80^{o}C to remove the entrapped air, which then was blended with the appropriate stoichiometric amounts of NMA hardener and BDMA accelerator (based on the amount of DGEBA and the masterbatch) for 15 min. The nanomodified resin was afterwards poured into release-coated silicon moulds (plate, cubic and cylindrical shapes) and degassed in the vacuum oven before curing to remove any air entrapped in the mixture. Finally, the resin system was pre-cured at 80^{o}C for 2 h, cured at 120 ^{o}C for 3 h and post-cured at 150 ^{o}C for 4 h with a ramp rate of 1^{o}C/min followed by cooling down to room temperature at 1^{o}C/min.

2.2 Transmission electron microscope (TEM)

The degree of dispersion of the silica nanosphere particle in the epoxy matrix was investigated using a TEM. TEM samples with a thickness of 85 nm were prepared using a Leica UC2 Ultra-microtome machine at room temperature. After cutting, sections were collected on 200-mesh copper grids. The specimens were examined using a FEI Tecnai TEM at an accelerating voltage of 80 kV. The images were captured using a Gatan MS600CW high resolution digital camera and collected using Gatan digital micrograph software at three different magnifications, 22500x, 115000x and 225000x.

2.3 Density measurement

Density of the cured epoxy is measured by the Archimedes principle in distilled water using a density balance. The tests were conducted according to ASTM standard D792. Three specimens were measured for each system.

2.4 Thermogravimetry analysis (TGA)

TGA is used to measure the weight change of a cured resin as it is heated at a controlled rate and in a controlled environment. The test was conducted according to ASTM standard E1131 using a Perkin Elmer TGA. The percentage of weight loss against heating temperature data were recorded by TGA PYRIS software. A sample mass of 15 to 30 mg was heated from room temperature to 800°C at a heating rate of 10°C/min in air at 50 ml/min to burn off the resin. The residue left after combustion was the silica nanoparticles. Three specimens were tested for each system. The volume fraction of the nanosilica in the epoxy was calculated using the equation given in ASTM standard D3171.

2.5 Compression test

Static uniaxial compression tests were carried out on cylindrical specimens using a Hounsfield universal testing instrument with a cross head speed of 1 mm/min. At least five specimens were tested for each system. The specimen dimension of 1:1 length to diameter (L/D) ratio (10 mm/10 mm), as recommended in [25], was selected. This helped to avoid buckling, reduce friction due to small cross-section area, avoid premature failure due to sharp corners and prevent self-reaction of the epoxy resin during curing. Cured resin was darkened

for thick specimens. In order to have smooth parallel ends perpendicular to the cylindrical axis, the cast specimens were machined on a lathe and polished to an accuracy of 0.01 mm (measured with a micrometer). All specimens were dried in a vacuum oven before being kept in vacuum at room temperature. Compression tests were also conducted on the 12.5x12.5x25.4 mm^3 cube specimens (according to ASTM standard D695) to study the effect of specimen geometry and dimensions on the compressive stress-strain response and their failure mechanisms.

In order to minimize the frictional forces between test machine platen and specimen loaded surfaces especially at circumference edges where barrelling may be triggered, the specimen ends were smeared with petroleum jelly. The compliance of the testing machine for compression, based on a technique proposed in [26], was performed to calculate the actual displacement of the specimen. In the 'direct technique' demonstrated by Kalidindi *et al* [26], the load-displacement relationship for the machine was measured without any specimen between the compression bars. The actual deformation of the sample can then be calculated by subtracting the non-sample displacement of the testing fixture from the total displacement recorded by the actuator. This load-displacement relationship for the machine can be used to correct the recorded load–displacement data for any specimen tested under uniaxial compression by the testing machine at the same crosshead speed.

The change in cross-sectional area is significant when calculating stress of polymer material loaded in compression. The stress was calculated using the current cross-sectional area (true stress) instead of the initial cross-sectional area (engineering stress). The true and engineering compressive stress-strain curves were compared in Fig. 1. The cross sectional area of the specimen increased with the compressive strain and therefore the true stress-strain curve plot showed lower values than the engineering curve. Fig. 1 shows the deformation of a typical specimen at different compressive strains over the corresponding true stress–strain curve. It can be seen that the barrelling effect of the specimen during compression (after the yield strain or even at higher strains before the fracture) was effectively minimised due to reduced friction. The compressive properties such as elastic modulus, strength, failure strain, yield strength and strain at yield point, were determined based on ASTM standard D695.

2.6 Scanning Electron microscope (SEM)

The post-failure surfaces of the compression specimens were observed using an SEM. All surfaces were coated with a thin layer of gold at 20 mA and 0.05 torr pressure using a Sputter

coater unit EMSCOPE SC500A before analysis to prevent charging. A CAMSCAN SEM was used to identify fracture mechanisms of the epoxy system at magnifications 20x–3500x with setting of accelerating voltage 10 kV and resolution 5.

3. Results and discussion

3.1 Distribution of nanosilica in the epoxy

Homogeneous dispersion of nanofillers in epoxy is a major challenge for fabricating nanocomposites. Agglomeration of nanoparticles (usually in micrometer or submicrometer size lumps) often gives adverse effects on the thermal and mechanical properties of the epoxy. This kind of badly fabricated composite does not represent the properties of a desired nanocomposite. In this study, a uniform distribution of nanosilica in Epikote 828 was achieved supported by the TEM migrographs presented in Fig. 2. There was no agglomeration of the SiO_2 nanoparticles even at high volume fraction (see Fig. 2b); the spherical shape silica nanoparticles have a mean particle size of 20 nm. Since the TEM slice is approximately 85 nm thick these TEM images do not reflect the actual volume fraction of nanosilica in the matrix. The volume fraction of the nanosilica was therefore measured using thermo-gravimetry analysis (TGA) that is discussed in the following section.

3.2 Volume fraction of nanosilica in the epoxy

Table 1 summarises physical properties of nanosilica-filled Epikote 828 as compared to the pure resin. A density of 1.22 g/cm^3 was measured for the unmodified Epikote 828. The measured density was found to increase with the nanosilica content (see Table 1). The increase in density is expected because the density of silica, ρ_{si} = 1.8 g/cm^3, is greater than that of the epoxy matrix. The inclusion of 25 wt% nanosilica increased the density of the epoxy for about 12%. The measured density was compared to the theoretical prediction based on the rule of mixtures. A slightly lower predicted density value was observed at higher nanosilica content as shown in Table 1.

TGA was conducted on the cured resin to confirm the weight fraction of nanosilica in the Epikote 828. Fig. 3 shows typical TGA results that illustrate the thermal degradation of nanomodified resin compared to the neat resin. All samples started to decompose at about 390^{o}C and completely decomposed at about 715^{o}C. The TGA profile illustrates four

decomposition mechanisms as shown in Fig. 3a. Stage A shows that the initial weight loss of about 0.1 wt.% occurred due to moisture content or water vaporization. Stage B represents decomposition of nanomodified and neat epoxy resins in air at temperature 390^{o}C-550^{o}C. Stage C shows decomposition of the carbon residues by oxidation at temperature 550-715^{o}C. The maximum degradation temperature of the epoxy resins and carbon residues was identified by the peak of the rate of weight loss versus sample temperature curve as shown in Fig. 3b(i) and 3b(ii), respectively, and summarized in Table 1. It was found that the thermal degradation of nanomodified epoxy and its carbon residue was higher compared to the pristine epoxy. For instance, the addition of 5 wt% nanosilica into the epoxy matrix increased the maximum degradation temperature of epoxy resin by 10^{o}C and that of carbon residue by 42^{o}C compared to the neat resin. This suggests that the nanofiller-matrix interfacial bonding is very strong and therefore higher temperature is needed to remove the epoxy which is stuck on the particle surface. Stage D shows the weight percentage of the remaining ash after the matrix is burnt off. The material remaining behind after exposing the sample to oxygen is the silica nanofiller. The TGA curve of the neat resin shows that the remaining residue is 0%. The average weight fraction and volume fraction of nanosilica in Epikote 828 is summarized in Table 1. The results showed that the average weight fraction of nanosilica in epikote 828 was 5 wt%, 13 wt% and 25 wt%. Thus, the volume fraction of nanosilica in the epoxy resin was 3.5 vol%, 9.4 vol% and 18.9 vol%, respectively.

3.3 True compressive stress-strain behaviour

In tension, cured epoxies failed at a very low tensile strain, e.g, about 8% strain at break as tested in [24]. However, in compression they exhibited a large plastic deformation, eg., up to 43% failure strain for pure Epikote 828 as shown in Fig. 1. The true stress-strain curve, as illustrated in Fig. 1, shows that epoxy undergoes elastic (region A) and plastic (region B) behaviour before rupture. The stress initially increases proportionally to the strain, obeying the Hooke's law, until it reaches an elastic limit (point C). The compressive modulus of the epoxy was calculated at 1% compressive strain. With an increase in the load beyond the proportional limit, the strain begins to increase more rapidly for each increment in stress until it reaches yield stress (point D) where the material deforms without an increase in the applied force. After yielding, the shortening increases with decrease in the applied load, known as plastic strain softening (region E), until the graph becomes plateau (shortening occurs with no noticeable increase in the compressive stress; see region F). As the material undergoing large

softening strains, the cross-sectional area is continually increasing resulting in increased resistance of the material to further deformation. Thus after region F, additional shortening requires an increase in the compressive load, known as plastic hardening mechanism (region G), until it reaches maximum load where the material rupture occurs (known as ultimate stress, point H).

The effect of nanosilica on the true compressive stress-strain response of the epoxy polymer was illustrated in Fig. 4. It can be seen that the presence of nanosilica enhanced the compressive stress-strain behaviour of the epoxy polymer. The addition of rigid microfillers or agglomerated nanofillers into epoxy resins commonly increases the stiffness but gives detrimental effect on the strain to break [10, 12, 15, 20-22]. Moreover, the strength of the composites is also reduced as the amount of these fillers increase. This is due to the high local stress concentration which leads to premature failure. Other than that, reduction in strength and failure strain demonstrated that the load transfer between matrix and particles is insufficient and the interface is weak. In contrast, Fig. 4 shows that the incorporation of nanosilica increased the compressive modulus and strength without reducing its failure strain even at high nanosilica content. A rigid silica nanoparticle has a Young's modulus of 70 GPa [23] while the neat Epikote 828 has an E=3 GPa. The presence of nanosilica improved ductility and promoted higher plastic hardening behaviour after yielding of the epoxy without reducing its strain to failure. This suggests that the rigid nanoparticles introduce additional mechanisms of energy absorption during compression. This gives a higher resistance against deformation which results in higher compressive stress and plastic hardening. In addition, the homogeneous dispersion of these high stiffness nanofillers in the matrix enhanced the fracture toughness of the system (larger area under stress-strain curve, see Fig. 4).

3.4 Compressive properties

The compressive properties of nanosilica-filled Epikote 828 are summarised in Table 2. It was found that the addition of nanosilica improved the compressive properties of the epoxy. For instance, the addition of 13 wt% nanosilica into the epoxy matrix enhances the compressive modulus by 19% and compressive strength by 58% with no significant changes in yield stress and failure strain. The highest content of nanosilica in the epoxy (25 wt%) gave a tremendous increase in compressive modulus and strength of more than 30% and 70%, respectively, compared to the neat polymer. This suggests that the nanofiller-matrix

interaction is very favourable and therefore stresses are efficiently transferred via the interface, which leads to higher strength compared to the pristine polymer.

3.5 The effect of specimen's shape and geometry

The compression tests were also conducted on prismatic specimens to study the effect of specimen's shape and geometry on the compressive properties of filled and unfilled epoxy. Table 2 shows the comparison between the compressive properties of cylindrical and cubic specimens. It was found that both have a similar Young's modulus, however, the measured compressive strength and failure strain of the cube type specimens were significantly lower than those of the cylindrical specimens, Table 2.

The deformed cylindrical and prismatic specimens during compression are illustrated in Figures 1 and 5, respectively. In theory, the specimen subjected to compression would get shorter and expand uniformly along its length (see Fig. 6a). However this could be achieved if there was zero friction between the flat ends of the specimen and the compression platens. In practice, it is difficult to completely eliminate friction. This results in barrelling formation where the ends of the specimen do not expand as much as its central region (see Fig. 6b). Compression tests on cylindrical specimens, Fig. 1, developed less barrelling deformation in addition to lower stress concentration near the loading ends when compared to prismatic ones, Fig. 5. These two effects resulted in higher failure loads for the cylindrical specimens, Fig. 4. The prismatic specimens failed prematurely due to buckling, which was triggered by longitudinal cracking that formed at specimen's edges (sharp corners) near the loaded ends.

Fig. 5 shows typical true stress-strain curves of prismatic specimens which were loaded in compression. The strain to failure and compressive strength of the pristine polymer were relatively lower than those of the nanomodified polymer. The resistance to plastic deformation of the nanomodified resin is higher compared to the pure resin system due to the presence of rigid nanoparticles. The true stress-strain response especially in the plastic region cannot be determined accurately. Compressive stress of cylindrical specimens was higher than that of the cube specimens at the same compressive strain. For example, the compressive stress of 25 wt% nanosilica system at 30% compressive strain was 184 MPa for the cylindrical specimen compared to 167 MPa for cube specimen. This discrepancy occurs because of the non-uniform deformation of the prismatic specimen which results in a complex stress state.

3.6 Morphology of fracture surface

For both cylindrical and prismatic specimens, the increase of the area under the stress-strain curve of the nanomodified polymer suggests improvement in fracture toughness when compared to the neat polymer. Fig. 7a shows the prismatic specimens after compression where the failure of the specimens was via barrelling and longitudinal cracking. SEM examination of the fracture surfaces, from the compression experiments, of neat Epikote 828 and nanomodified epoxy can provide detailed information on the cause and location of failure and, hence, explain the reasons for the increase in energy absorption of nanocomposites. The fracture surface of neat and modified epoxy samples can be roughly divided into two regions: crack initiation zone (high stress concentration region) and crack propagation zone (crack growth region) as shown in Fig. 7b. There are various toughening mechanisms such as crack pinning, particle bridging, crack path deflection, particle yielding induced shear banding and microcracking [9, 12-13, 15-17] which have been used to explain the energy-dissipative mechanisms of the rigid particle filled epoxy systems loaded in various types of loadings. Among these, crack deflection, filler/matrix debonding, shear yielding, shear banding and step formations have been proposed as applicable for nanoparticles modified epoxy systems [23, 24, 27, 28].

Examination of the fracture surface of pure polymer showed a relatively smooth and glassy surface (brittle-like failure) compared to that of the nanomodified polymer which demonstrates large scale plastic deformation of the matrix, as shown in Fig. 8. The crack deflection toughening is created when the crack front approaches an obstacle, such as nanoparticles, and it is tilted and even twisted out of its original plane. This alters the stress state near crack tip, produces non-planar cracks, increases fracture surface roughness and consumes additional fracture energy. In addition, a further energy absorption mechanism is based on the increase of the matrix plasticity. Shear yielding of the matrix leads to the formation of shear bands. It can be seen that the nanomodified polymer shows a textured surface when compared with the mirror-like fracture surface of the pure epoxy. These mechanisms contribute to a tougher system.

3.7 Prediction of compressive modulus

The elastic response of most polymer matrices is usually similar in tension and compression, and therefore the compressive elastic modulus of the studied systems was

estimated using various models suggested and reviewed in [29-35]. Table 3 summarises several theoretical models that are commonly used to predict the modulus of elasticity of particle-modified polymers. These are rule of mixtures, Halpin-Tsai [31, 32] and Lewis-Nielsen [29, 33-35] models. The theoretical predictions of compressive modulus were compared to the measured values as shown in Fig. 9. It was found that most of the prediction curves were in a good agreement with the measured data, where the compressive modulus increases with the nanosilica content. The upper bound rule of mixtures equation gives poor prediction when compared to the present experimental data. The Halpin-Tsai model includes the shape factor of the filler particle. For the case of spherical particles used in the present work, the length of the particle w equals the thickness of the particle t and therefore the shape factor $\zeta=2w/t=2$. For a low volume fraction of the nanofiller, the Halpin-Tsai prediction gives a very good agreement with the experimental data. However, when the silica nanoparticle content is more than 5 vol% the prediction curve lies above the measured values.

The Lewis-Nielsen model takes into account the degree of dispersion of particles in the matrix, V_{max} and the particle-matrix adhesion, k_E. Fig. 2 shows no agglomeration of the nanosilica particles therefore for random close packing and non-agglomerated spheres, $V_{max}=0.632$ was used in the calculation. Other than that, Fig. 4 shows that the compressive strength of nanomodified system was higher than that of the pure polymer. This suggests a very strong nanofillller-matrix interfacial adhesion that helps the load to be effectively transferred via the interface. Therefore, a perfect adhesion of $k_E=2.167$ was assumed in the non-slip Lewis-Nielsen model. This model gives the best agreement to the measured values when compared with the other models. However, at a very high nanofiller content (more than 19 vol%) the measured compressive modulus is lower than the predicted value. This is a common observation, since the model assumes that there is perfect bonding between the particles and the matrix, which may not be the case at very high filler content. This is due to the fact that some particle agglomeration may occur at high filler content in addition to particle slippage and imperfect adhesion.

4. Concluding remarks

A series of nanocomposites was developed based on nanosilica and Epikote 828 epoxy resin. TEM micrographs revealed that well-dispersed and non-agglomerated nanocomposite systems were produced. The volume fraction of silica nanoparticles in the matrix of 3.5 vol%, 9.4 vol% and 18.9 vol% was determined using the TGA. The degradation temperature

nanomodified epoxy was slightly higher than that of the unreinforced polymer. This suggests that the interfacial adhesion between particle and matrix is very good. The performance of the nanocomposites was evaluated via static uniaxial compression tests. Nanocomposites offer higher compressive stiffness and strength when compared to the neat polymer without sacrificing the material's strain to failure. The predicted modulus of elasticity using the Lewis-Nielsen model showed a very good agreement when compared to measured values. In addition, the true compressive stress-strain response showed that the presence of nanosilica improves ductility and promotes higher plastic hardening behaviour after yielding. The nanoparticles enhanced the shear deformation of the matrix and thus influence the crack propagation due to the formation of shear bands. This contributes to a tougher system. The nanomodified resin is a promising candidate for developing nanosilica-filled carbon fibre reinforced polymer composites with the aim of improving their matrix dominated properties. This will provide more damage resistant and tolerant composite structures [36] especially when loaded in compression and in compression after impact.

Acknowledgements

The authors gratefully acknowledge the Ministry of Higher Education Malaysia for a PhD scholarship of Mrs A Jumahat. Also, they would like to thank Nanoresins AG, Geesthacht, Germany for the supply of materials and technical supports. The authors wish to express their gratitude to the University of Sheffield Composites Group members, especially Dr S Hayes, Dr P Bailey, Dr T Swait and A D Lafferty for useful technical discussions.

References

[1] Soutis C (2005) Progress in Aerospace Sciences 41(2):143-151.

[2] Mallick PK (1988) Fiber-reinforced composites. Marcel Dekker Inc, New York.

[3] Jang BZ (1994) Advanced polymer composites: principles and applications. ASTM International, USA.

[4] Jumahat A, Soutis C, Jones FR, Hodzic A (2010) Composite structures 92(2):295-305.

[5] Bagheri R, Pearson RA (2000) Polymer 41:269-276.

[6] Lu R, Plummer CJG, Cantwell WJ, Kausch HH (1996) Polymer Bulletin 37:399-406.

[7] Recker HG, Altsaedt V, Tesch H, Weber T (1997) Toughened, fibre-reinforced thermosetting resin matrix prepregs and composites made therefrom. United States Patent 5627222. US patents, USA.

[8] Mimura K, Ito H, Fujioka H (2001) Polymer 149:9223-9233.

[9] Cardwell BJ, Yee AF (1998) Journal of Materials Science 33:5473-5484.

[10] Cano RJ, Dow MB (1992) Properties of five toughened matrix composite materials. NASA technical paper 3254. NASA Langley research centre, USA.

[11] Day RJ, Lovell PA, Wazzan AA (2001) Composites Science and Technology 61:41-56.

[12] Lee J, Yee AF (2001) Journal of Materials Science 36:7-20.

[13] Bagheri R, Pearson RA (1995) Polymer 36(25):4883-4885.

[14] Frohlich J, Kautz H, Thomann R, Frey H, Mulhaupt R (2004) Polymer 45:2155-2164.

[15] McGrath LM, Parnas RS, King SH, Schroeder JL, Fischer DA, Lenhart JL (2008) Polymer 49:999-1014.

[16] Kinloch AJ, Yuen ML, Jenkins SD (1994) Journal of Materials Science 29:3781-3790.

[17] Pearson RA, Yee AF (1993) Polymer 34(17):3658-3670.

[18] Babayan EP, Nguyen HX (1994) Epoxy matrix containing amine hardener and micropulverized polyimide. United States Patent 5310825. US patents, USA.

[19] Parlevliet PP, Bersee HEN, Beukers A (2007) Journal of Composites Part A 38:1581-1596.

[20] Zhou G (2007) Preparation, structure, and properties of advanced polymer composites with long fibers and nanoparticles. PhD thesis. The Ohio State University.

[21] Yasmin A, Luo JJ, Abot JL, Daniel IM (2006) Composites Science and Technology 66:2415–2422.

[22] Gojny FH, Wichmann MHG, Köpke U, Fiedler B, Schulte K (2004) Composites Science and Technology 64(15):2363-2371.

[23] Johnsen BB, Kinloch AJ, Mohammed RD, Taylor AC, Sprenger S (2007) Polymer 48:530-541.

[24] Rosso P, Ye L, Friedrich K. Sprenger S (2006) Journal of Applied Polymer Science 100:1849-1855.

[25] Behzadi S, Jones FR (2008) Composites Science and Technology 68:2690-2696.

[26] Kalidindi SR, Abusafieh A, EI-Danaf E (1997) Experimental Mechanics 37(2):210-215.

[27] Ma J, Mo MS, Du XS, Rosso P, Friedrich K, Kuan HC (2008) Polymer 49:3510-3523.

[28] Zhang H, Tang LC, Zhang Z, Friedrich K, Sprenger S (2008) Polymer 49:3816-3825.

[29] Nielsen LE, Landel RF (1994) Mechanical properties of polymers and composites. Marcel Dekker Inc, New York

[30] Ahmed S, Jones FR (1990) Journal of Materials Science 25:4933-4942.

[31] Halpin JC (1969) Journal of Composite Materials 3:732-734.

[32] Halpin JC, Kardos JL (1976) Polymer Engineering and Science 16(5):344-352.

[33] Nielsen LE, Lewis TB (1970) Journal of Applied Polymer Science 14(6):1449-1471.

[34] Nielsen LE (1967) Journal of composite materials 1:100-119.

[35] McGee S, McCullough RL (1981) Polymer Composites 2(4):149-161.

[36] Soutis C (2009) Plastics, Rubber and Composites: Macromolecular Engineering 38:359-366.

Figure
Click here to download Figure: Figures_J Mat Sci_ A Jumahat_Rev1.doc

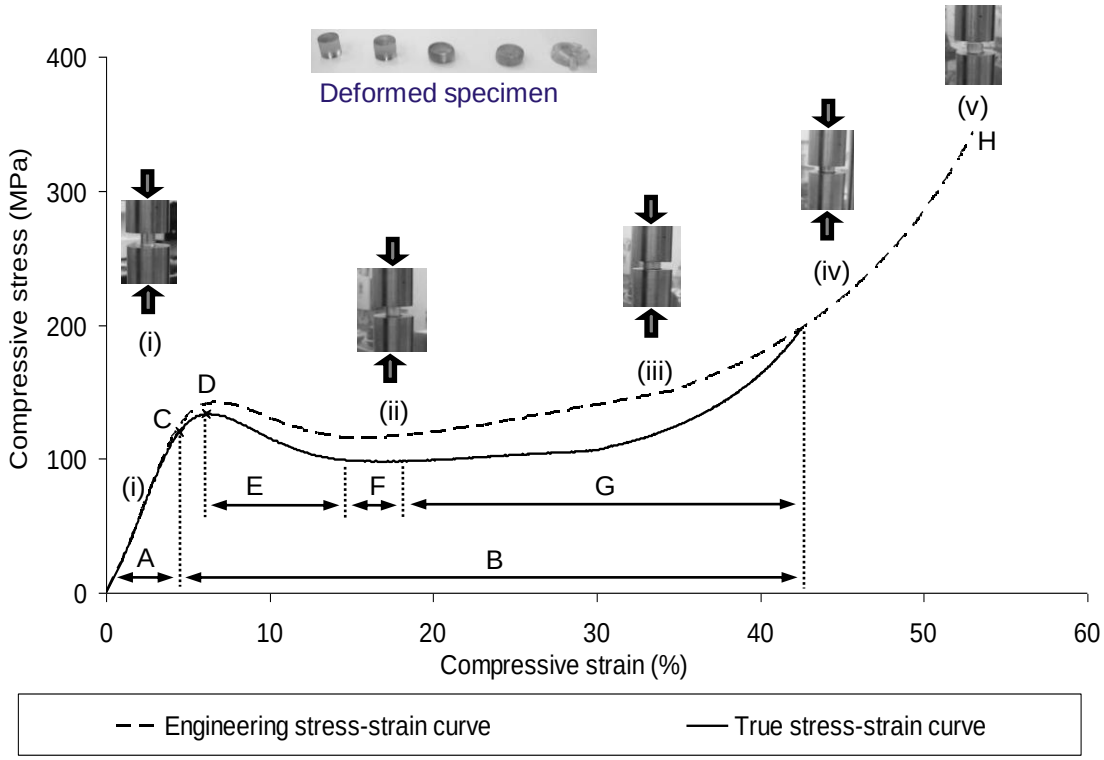

Fig. 1. Typical engineering and true stress-strain curves of cylindrical specimen of pure Epikote 828 loaded in static uniaxial compression. (i), (ii), (iii), (iv) and (v) show the deformation of a typical specimen in between the compression rods at different compressive strains. A, B, C, D, E, F, G and H are the elastic region, plastic region, elastic limit, yield point, plastic strain softening region, plateau region, plastic strain hardening region and ultimate stress, respectively.

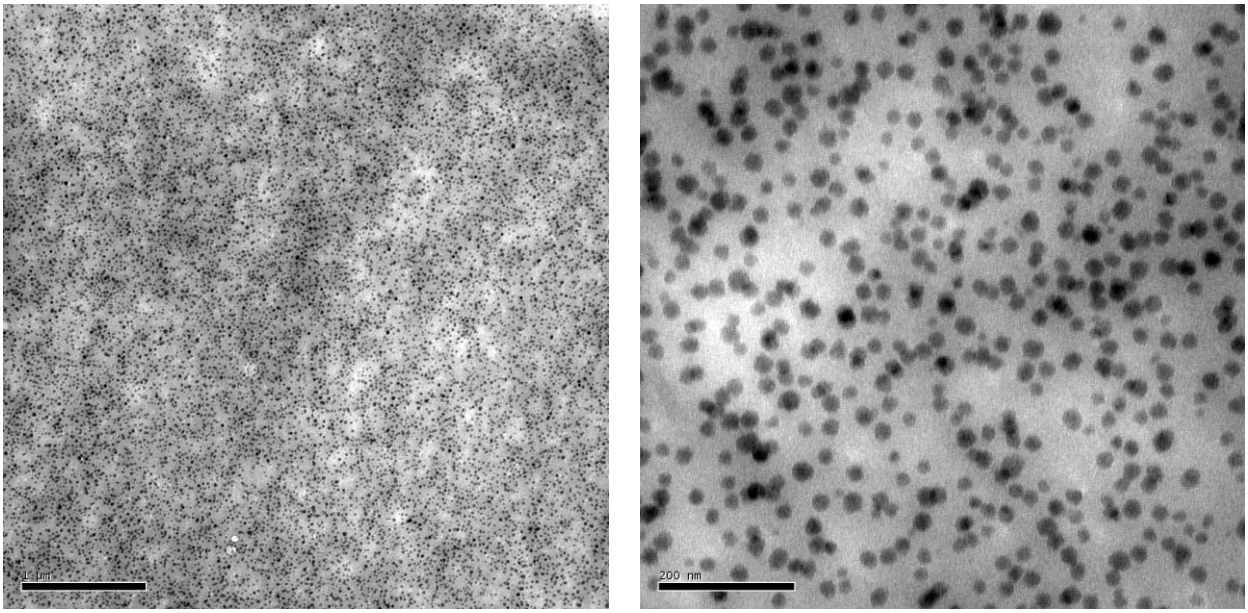

(i) (ii)

(a) 13 wt% nanosilica

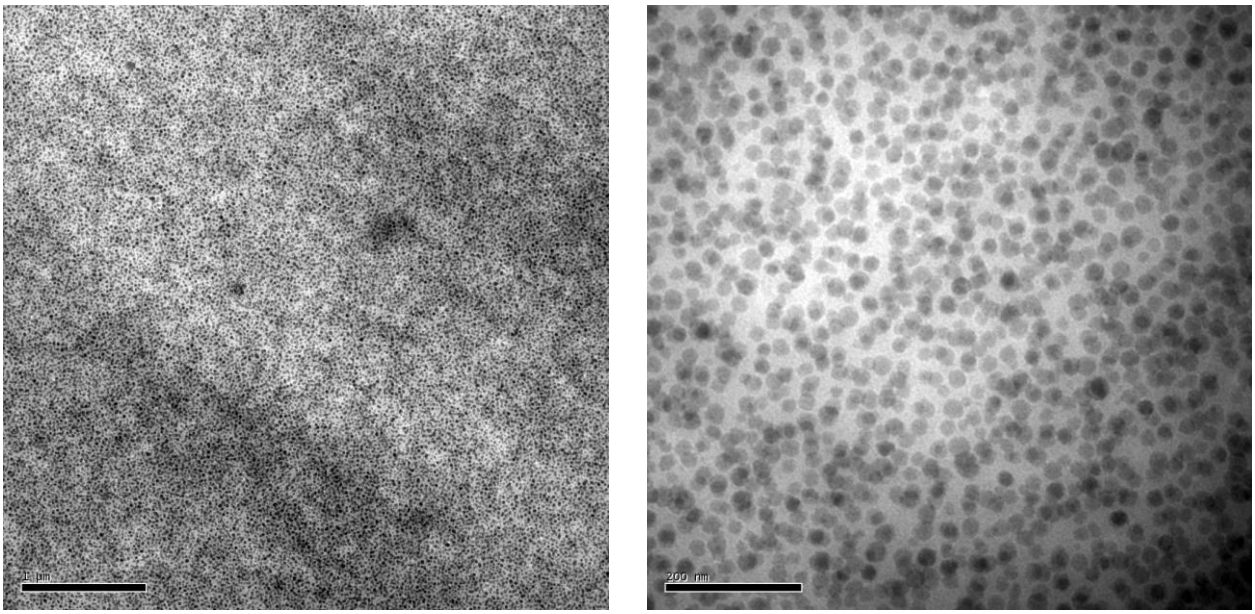

(i) (ii)

(b) 25 wt% nanosilica

Fig. 2. TEM micrographs showing a homogeneous dispersion of (a) 13 wt% and (b) 25 wt% nanosilica in Epikote 828 at (i) 22500x and (ii) 115000x magnifications. The spherical silica nanoparticles have mean diameter of 20 nm and maximum diameter of 50 nm.

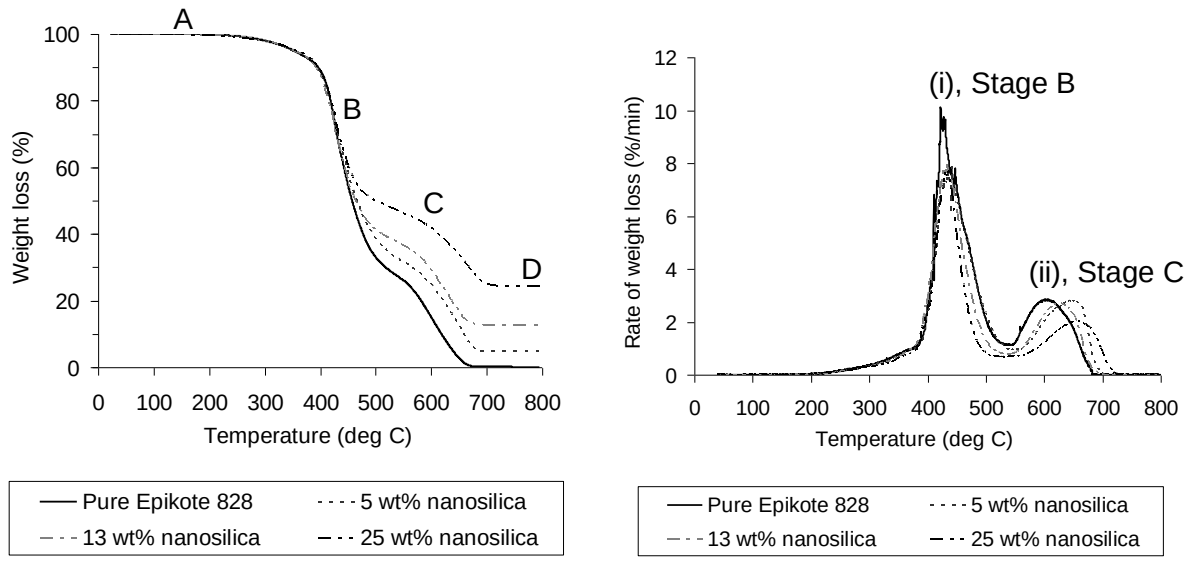

Fig. 3. Typical TGA results illustrating (a) percentage of weight loss and (b) rate of weight loss as a function of sample temperature.

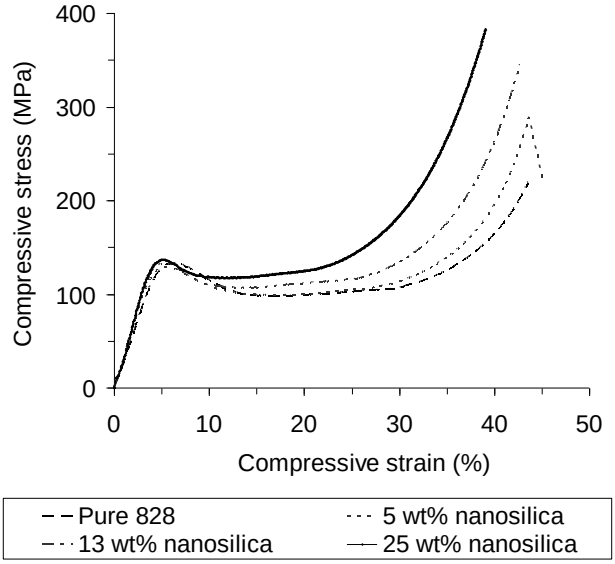

Fig. 4. Typical true stress-strain curves of cylindrical specimens loaded in static uniaxial compression showing the effect of nanosilica on the compressive stress-strain behaviour of Epikote 828.

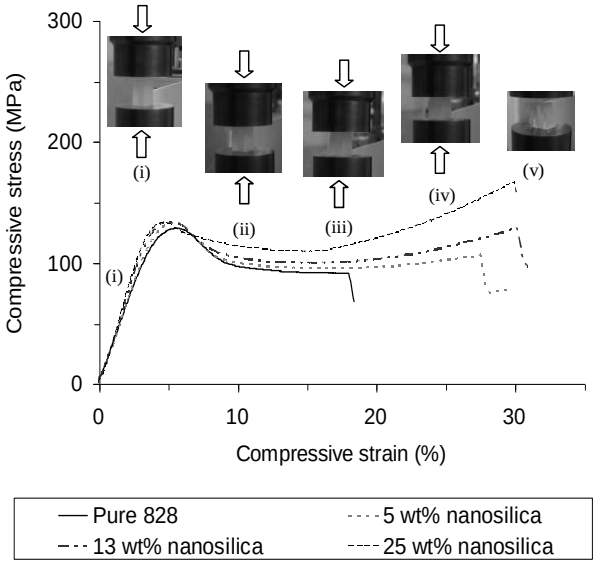

Fig. 5. Typical true stress-strain curves of prismatic (cube) specimens loaded in static uniaxial compression showing the effect of nanosilica on the compressive stress-strain behaviour of Epikote 828. (i), (ii), (iii), (iv) and (v) show the deformation of a typical specimen in between the compression rods at different compressive strains.

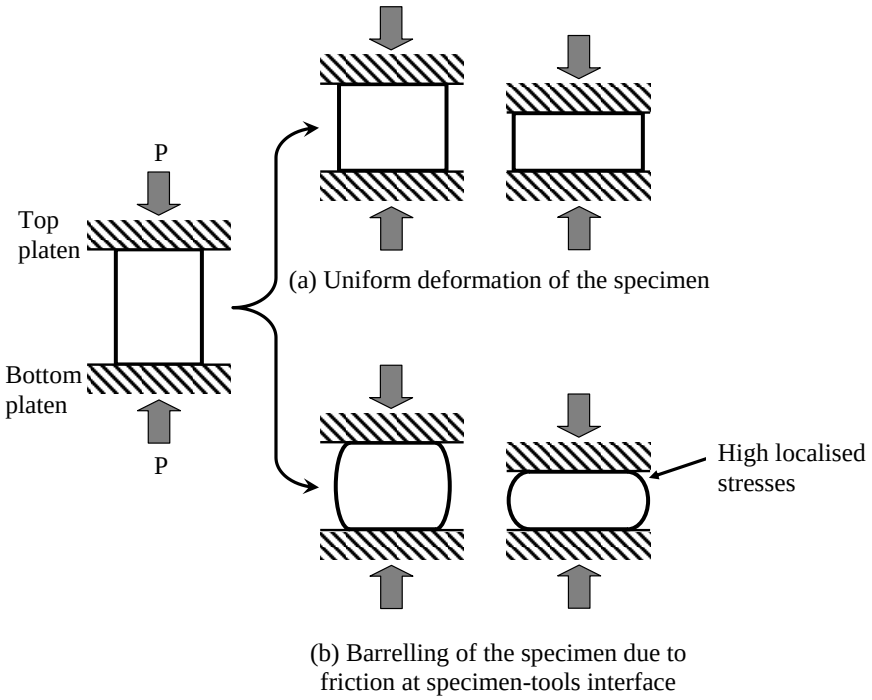

Fig. 6. Schematic diagram of epoxy polymer specimen loaded in compression showing (a) uniform and (b) non-uniform deformations; high localised stresses can develop leading to early damage and hence premature failure.

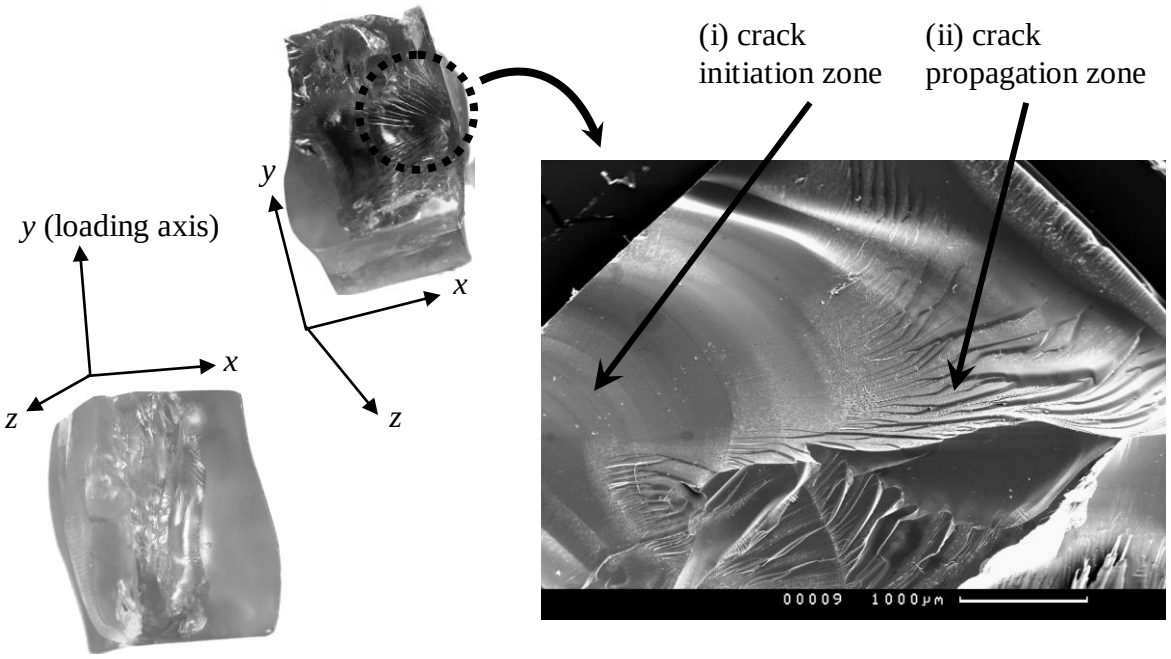

Fig. 7. (a) Axially loaded cube type specimens fail via barrelling and longitudinal cracking followed by buckling at higher loading and (b) SEM micrograph of the fracture surface showing crack initiation and crack propagation zones.

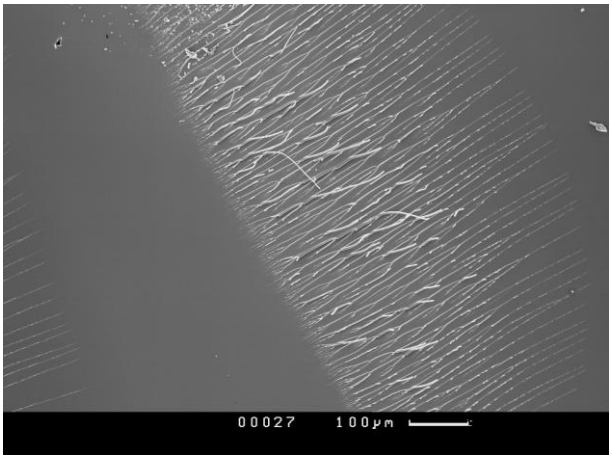

(i) crack initiation zone

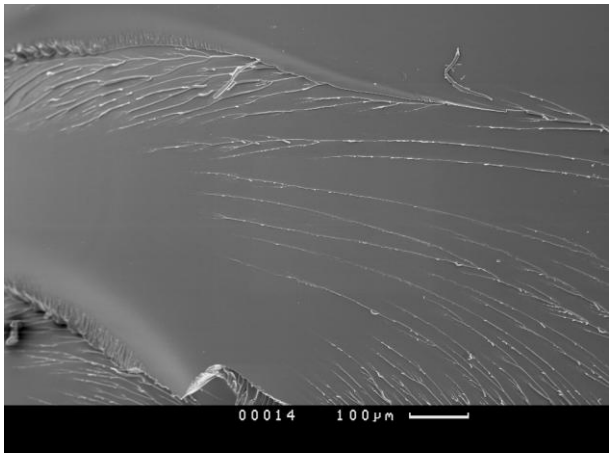

(ii) crack propagation zone

(a) Pure Epikote 828

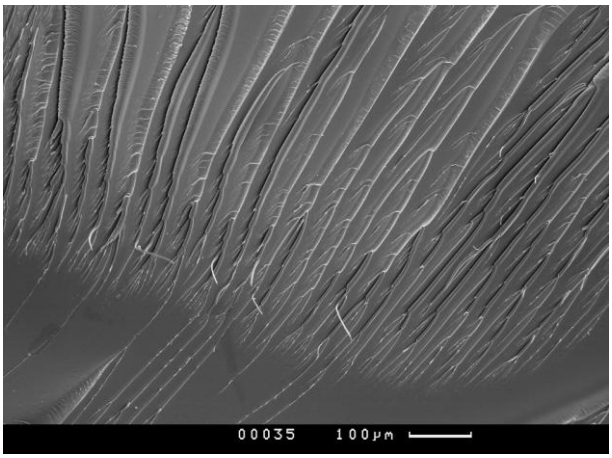

(i) crack initiation zone

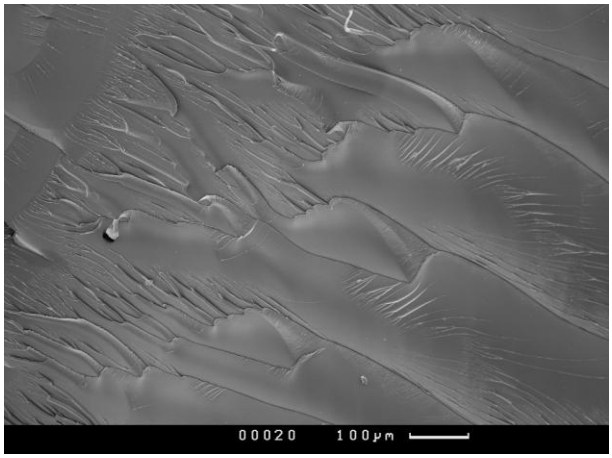

(ii) crack propagation zone

(b) 5 wt% nanosilica in Epikote 828

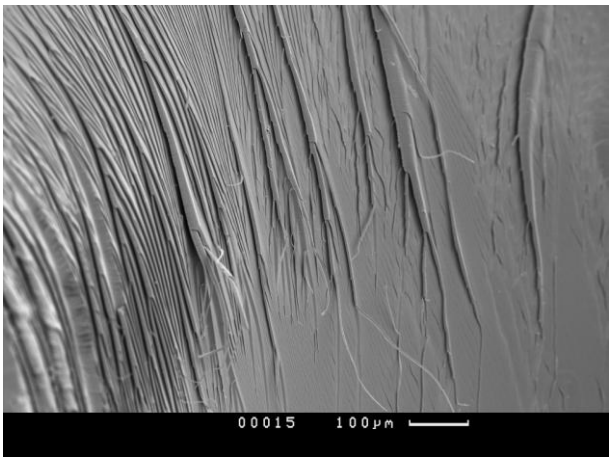

(i) crack initiation zone

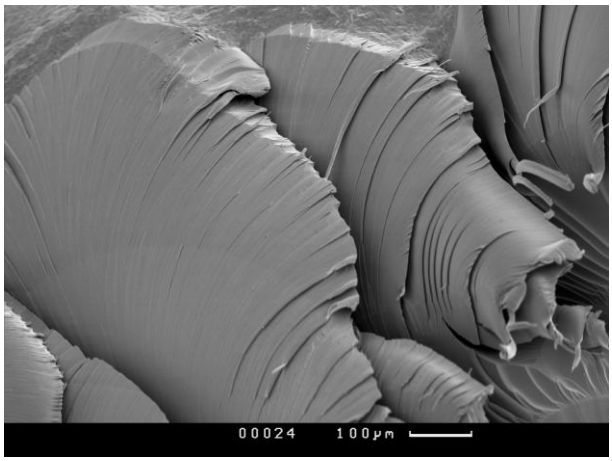

(ii) crack propagation zone

(c) 25 wt% nanosilica in Epikote 828

Fig. 8. SEM examination on fracture surface of cube type specimens after compression. Pure Epikote 828 (a) shows smooth fracture surface while nanocomposites (b and c) show large scale resin shear deformation that leads to the formation of shear bands. More textured surface is observed as the nanoparticle content is increased (c).

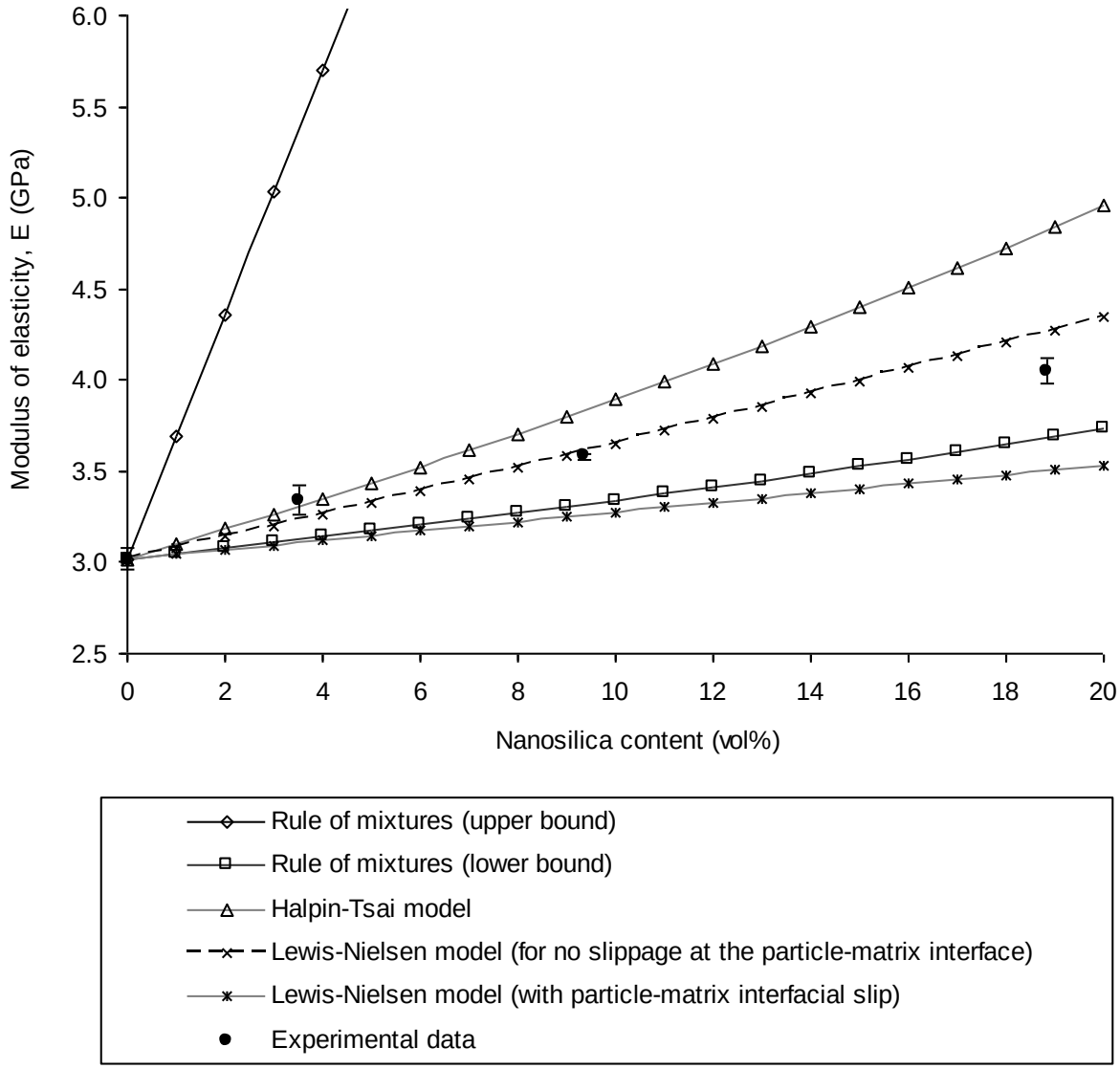

Fig. 9. Theoretical prediction of the compressive modulus of nanosilica-modified Epikote 828 in comparison with the measured data. All curves were calculated based on models and input data summarized in Table 3.

Table 1
Summary of density of nanosilica-filled Epikote 828 compared to the neat resin (measured using the density balance and predicted using the rule of mixtures) and determination of volume fraction of nanosilica in the Epikote 828 using the TGA method.

Physical properties	Nanosilica-filled Epikote 828 resin nanocomposites			
	pure	5 wt%	13 wt%	25 wt%
Density (measured by density balance) ρ_{nc} (g/cm^3)	1.221 ± 0.001	1.250 ± 0.002	1.296 ± 0.001	1.366 ± 0.001
Theoretical density (calculated using the rule of mixtures) $\rho_{nc}(g/cm^3) = \rho_{ep}V_{ep} + \rho_{si}V_{si}$	1.22	1.24	1.27	1.33
Maximum degradation temperature of epoxy resin (^{o}C)	424.34 ± 1.81	435.14 ± 2.59	430.48 ± 0.72	431.38 ± 1.06
Maximum degradation temperature of carbon residue (^{o}C)	605.69 ± 2.09	647.70 ± 1.41	631.99 ±1.64	654.59 ± 1.19
Weight fraction of nanosilica (wt%) (measured by TGA) W_{si} (%)	-	5.04 ± 0.09	13.02 ± 0.11	24.85 ± 0.25
Volume fraction of nanosilica (vol%) $V_{si}(\%) = W_{si} \times \frac{\rho_{nc}}{\rho_{si}}$ (where ρ_{si} = 1.8 g/cm^3)	-	3.50	9.37	18.86

Table 2
Effect of specimen's shape and geometry on the compressive properties of nanosilica-filled epoxy nanocomposites

Compressive property	Nanosilica-filled Epikote 828 resin nanocomposites							
	pure		5 wt%		13 wt%		25 wt%	
	Cyl.	Prism	Cyl.	Prism	Cyl.	Prism	Cyl.	Prism
Compressive modulus, E (GPa)	3.02 ± 0.06	3.12 ± 0.02	3.34 ± 0.08	3.39 ± 0.02	3.58 ± 0.02	3.60 ± 0.01	4.05 ± 0.07	4.04 ± 0.07
Compressive stress at yield, σ_y (MPa)	132.99 ± 0.20	126.59 ± 0.39	130.35 ± 0.31	130.93 ± 0.65	133.08 ± 0.39	131.80 ± 0.97	138.88 ± 0.84	130.75 ± 1.13
Compressive strain at yield point, ε_y (%)	6.50 ± 0.05	5.53 ± 0.03	5.70 ± 0.10	5.37 ± 0.04	5.46 ± 0.05	4.91 ± 0.11	5.12 ± 0.07	4.49 ± 0.06
Compressive strength, σ_u (MPa)	211.47 ± 3.17	126.59 ± 0.39	274.60 ± 22.66	130.93 ± 0.65	335.03 ± 13.35	131.80 ± 0.97	372.00 ± 7.64	158.69 ± 9.68
Compressive strain at break, ε_f (%)	42.66 ± 0.65	16.49 ± 1.56	39.74 ± 2.55	23.67 ± 2.40	42.17 ± 0.48	28.54 ± 1.57	38.89 ± 0.19	27.96 ± 1.34
Prism = prismatic or cubic shape specimen of 12.5 mm width x 12.5 mm thickness x 25.4 mm length Cyl. = cylindrical shape specimen of 10 mm diameter x 10 mm length								

Table 3
Prediction of compressive modulus of nanosilica-filled Epikote 828 nanocomposites using several types of theoretical models.

Theoretical models	Ref.	Eqn. and input data
Rule of mixtures	[30]	Upper bound, $E_{nc} = E_{si}V_{si} + E_{ep}V_{ep}$ Lower bound, $E_{nc} = \frac{E_{si}E_{ep}}{E_{si}V_{ep} + E_{ep}V_{si}}$ where E_{nc} = predicted nanocomposites modulus E_{ep} = modulus of the epoxy = 3.02 GPa E_{si} = modulus of the nanosilica = 70 GPa V_{ep} = volume fraction of the epoxy V_{si} = volume fraction of the nanosilica
Halpin-Tsai model	[31,32]	$E_{nc} = \frac{1+\zeta\eta V_{si}}{1-\eta V_{si}} E_{ep}$ where ζ =shape factor = 2 for spherical particles $\eta = \frac{\left(\frac{E_{si}}{E_{ep}} - 1\right)}{\left(\frac{E_{si}}{E_{ep}} + \zeta\right)} = 0.88$
Lewis-Nielsen model	[29,33-35]	$E_{nc} = \frac{1+(k_E - 1)\beta V_{si}}{1-\beta\mu V_{si}} E_{ep}$ where k_E = 2.167 if there is no slippage at the particle-matrix interface [18] k_E = 0.867 if there interfacial slip occur [23] $\beta = \frac{\left(\frac{E_{si}}{E_{ep}} - 1\right)}{\left(\frac{E_{si}}{E_{ep}} + (k_E - 1)\right)}$ $\mu = 1 + \frac{(1-V_{si})}{V_{\max}}\left[(V_{\max}V_{si}) + (1-V_{\max})(1-V_{si})\right]$ V_{max} = 0.632 for random close packing, non-agglomerated spheres [29]